Nuclear Engineering and Technology 54 (2022) 2213–2220

Contents lists available at ScienceDirect

Nuclear Engineering and Technology

journal homepage: www.elsevier.com/locate/net

Original Article

Performance prediction of gamma electron vertex imaging (GEVI) system for interfractional range shift detection in spot scanning proton therapy

Sung Hun Kim [a], Jong Hwi Jeong [a], Youngmo Ku [b], Jaerin Jung [b], Chan Hyeong Kim [b, *]

[a] Center for Proton Therapy, National Cancer Center, Goyang-si, 10408, Gyeonggi-do, South Korea
[b] Department of Nuclear Engineering, Hanyang University, Seoul, 04763, South Korea

ARTICLE INFO

Article history:
Received 10 July 2020
Received in revised form
23 November 2021
Accepted 20 December 2021
Available online 22 December 2021

Keywords:
Proton therapy
Beam range verification
Prompt gamma
Gamma electron vertex imaging

ABSTRACT

The maximum dose delivery at the end of the beam range provides the main advantage of using proton therapy. The range of the proton beam, however, is subject to uncertainties, which limit the clinical benefits of proton therapy and, therefore, accurate *in vivo* verification of the beam range is desirable. For the beam range verification in spot scanning proton therapy, a prompt gamma detection system, called as gamma electron vertex imaging (GEVI) system, is under development and, in the present study, the performance of the GEVI system in spot scanning proton therapy was predicted with Geant4 Monte Carlo simulations in terms of shift detection sensitivity, accuracy and precision. The simulation results indicated that the GEVI system can detect the interfractional range shifts down to 1 mm shift for the cases considered in the present study. The results also showed that both the evaluated accuracy and precision were less than 1–2 mm, except for the scenarios where we consider all spots in the energy layer for a local shifting. It was very encouraging results that the accuracy and precision satisfied the smallest distal safety margin of the investigated beam energy (i.e., 4.88 mm for 134.9 MeV).

1. Introduction

In proton therapy, most of the proton dose is focused at the end of the beam range, which makes proton therapy to be more attractive treatment modality compared to other conventional radiotherapies using photons and electrons. The range of the proton beam in the patient, however, is highly sensitive to errors such as anatomical inhomogeneity, anatomical change between fractions, and patient mispositioning. Furthermore, the prediction of the range also can be easily varied by CT conversion uncertainty, RBE variations, etc. [1]. Therefore, the patient safety is currently secured by using the safety margin and restricting the choice of beam angles [2], which consequently limits the clinical benefits of proton therapy. To fully exploit the clinical benefits of proton therapy, therefore, the proton range uncertainty should be minimized.

As an important methods to reduce beam range uncertainties, monitoring of beam range in the patient, so-called *in vivo* range verification, has been investigated using several modalities: ion-induced ultrasounds [3], spine MRI changes [4], secondary electron bremsstrahlung (SEB) [5], positron emission tomography (PET) [6], prompt gamma (PG) [7], etc. Among these modalities, PG detection has been pursued as promising due to the direct and instantaneous perception of the beam range [2,8–10], and accordingly, several PG detection systems have been proposed and developed based on different concepts: mechanical collimation [7,11,12], Compton imaging [13], prompt gamma timing (PGT) [14], prompt gamma peak integral (PGPI) [15], prompt gamma spectroscopy (PGS) [16], etc. These PG detection systems are gradually approaching the clinical use, and recently, knife-edge slit camera which employs the mechanical collimation was reached the clinical application [17,18].

In this context, we proposed a new PG detection concept, called 'gamma electron vertex imaging (GEVI),' aiming at application to spot scanning proton therapy [19]. In the GEVI method, the PGs from the proton interactions in the patient are converted to electrons by Compton scatterings in a thin beryllium plate, called as electron converter, and the Compton-recoiled electrons are subsequently traced by two hodoscopes and a calorimeter to identify the locations of the vertices of proton interactions in the patient. The main advantage of a GEVI system is that it does not require a

* Corresponding author.
E-mail address: chkim@hanyang.ac.kr (C.H. Kim).

https://doi.org/10.1016/j.net.2021.12.027

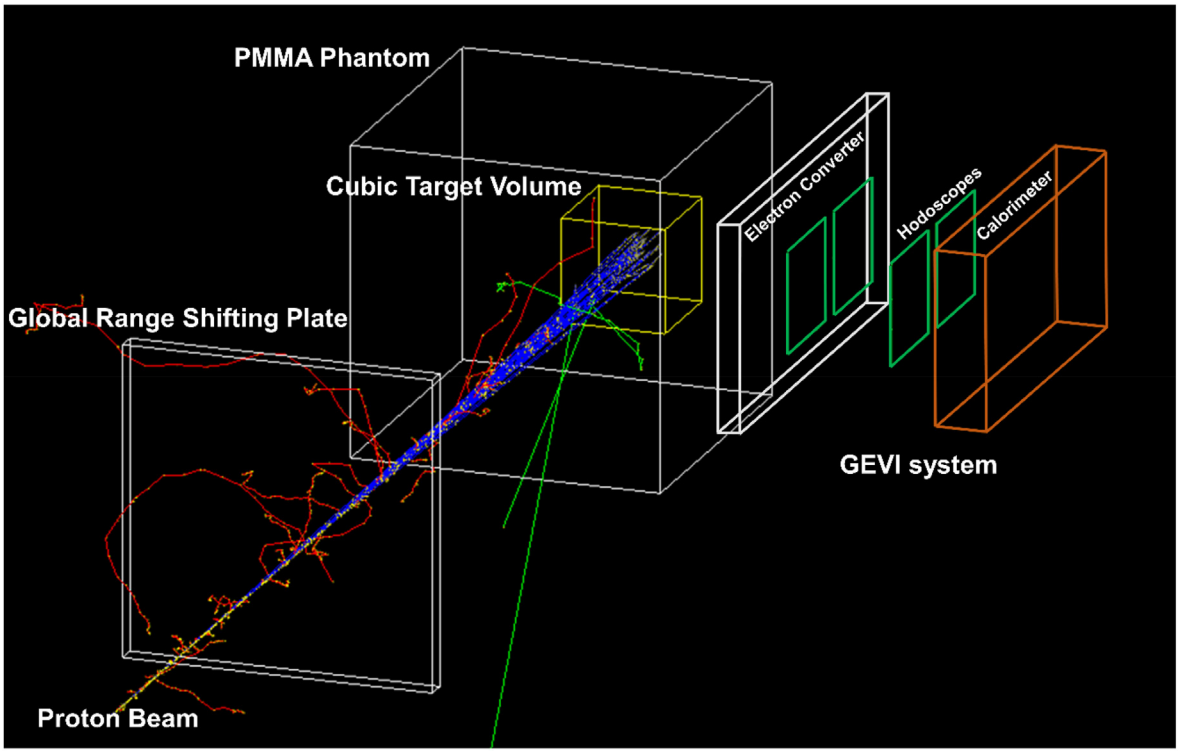

Fig. 1. GEVI system, PMMA phantom, global range shifting plate, and cubic target volume modeled in Geant4 Monte Carlo simulation. This example is for simulation of global range shifting for cubic target volume.

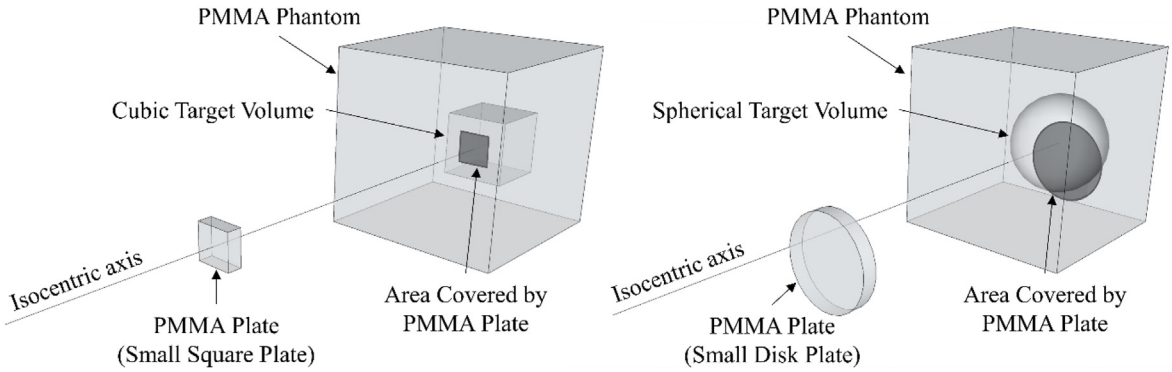

Fig. 2. Location of PMMA plate for local shift for cubic (left) and spherical (right) dose distributions.

massive collimation system and, therefore, can be made very light and compact. The GEVI method also provides a two-dimensional image, which might be useful in further verification of the treatment. Recently, a prototype of the GEVI system was constructed and its performance was evaluated for therapeutic proton beams [20]. These studies generally demonstrated the feasibility of the GEVI system, but the performance of the GEVI system was evaluated only for single-spot cases.

In the present study, the performance (i.e., shift detection sensitivity, accuracy and precision) of the GEVI system in spot scanning proton therapy was predicted for multi-spot cases by using Geant4 Monte Carlo simulations, and the results were analyzed with statistical hypothesis tests such as one-way ANOVA tests and one-sample t-tests. For this study, spot scanning proton treatments for two simple shapes (i.e., cubic, spherical) of dose distribution in a cubic polymethyl methacrylate (PMMA) phantom were planned with a treatment planning system, and the results were used to simulate the treatment with Geant4, considering both global and local shifting scenarios.

2. Materials and methods

2.1. GEVI system

The GEVI system consisted of an electron converter (200 mm (W) × 100 mm (H) × 10.8 mm (T) beryllium plate), two hodoscopes (100 mm (W) × 50 mm (H) × 150/300 μm (T) double-sided silicon strip detectors, DSSDs), a calorimeter (160 mm (W) × 85 mm (H) × 25 mm (T) plastic scintillation detector) and related signal processing and data acquisition systems. In the electron convertor, the PGs are converted to electrons by Compton scatterings. Two hodoscopes, subsequently, trace the

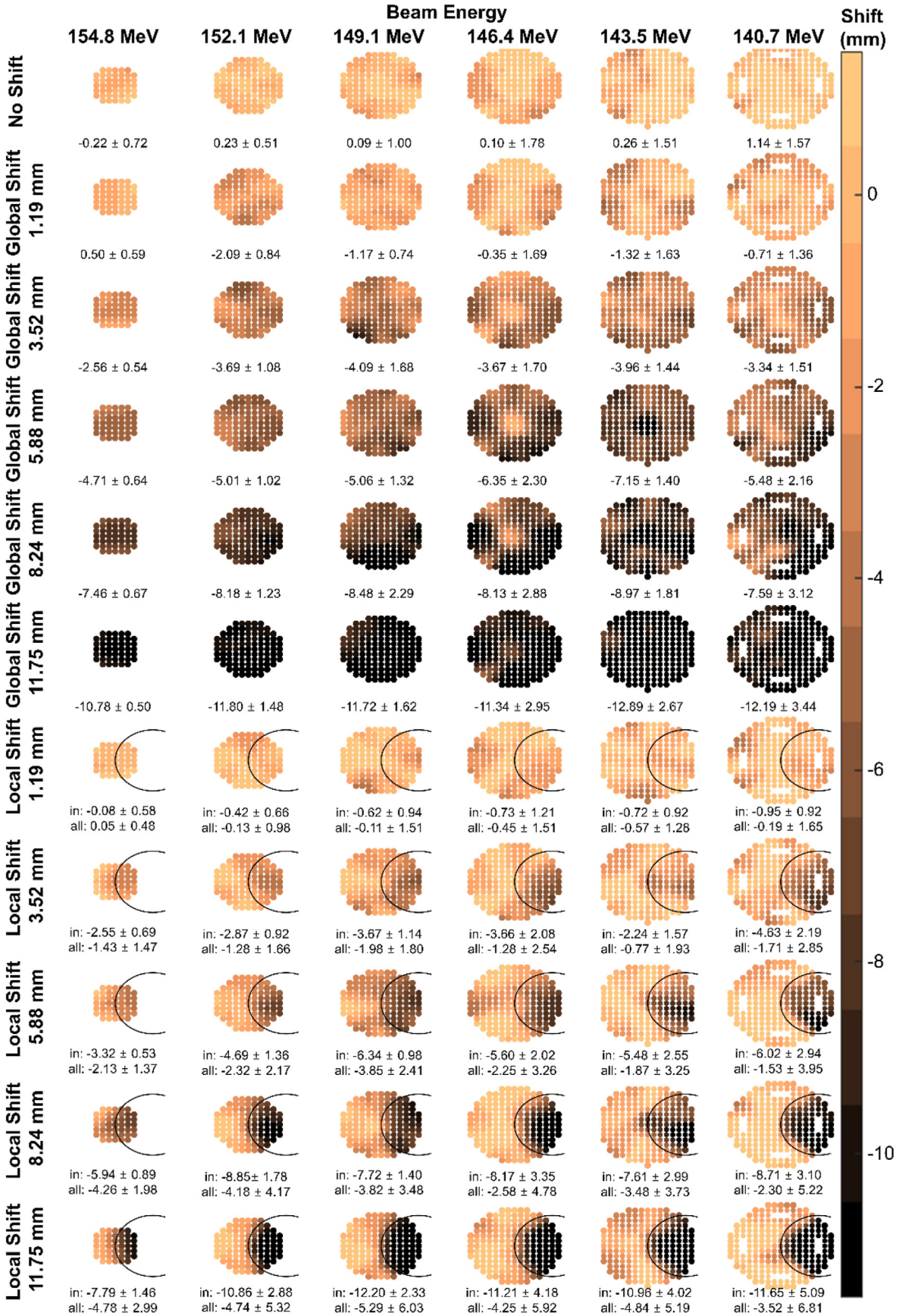

Fig. 3. Map of interfractional range shifts in the beam's eye view for spherical dose distribution estimated from Geant4 Monte Carlo simulations for the shifting scenarios. Spot sizes are proportional to the number of protons. The areas of local shift are marked with the black line. For each energy layer, the layer-averaged range shifts ± standard deviations (1σ) are given.

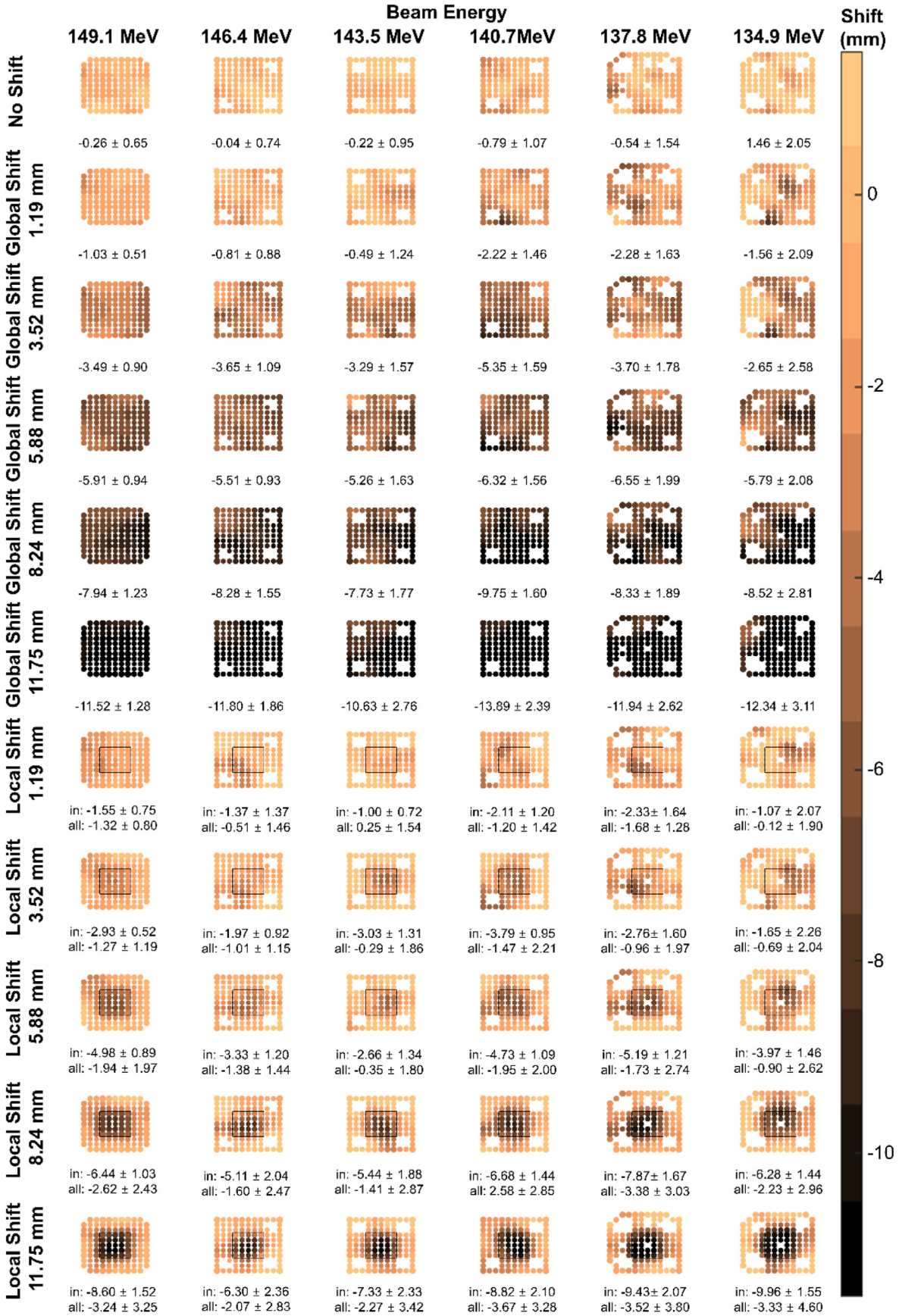

Fig. 4. Map of interfractional range shifts in the beam's eye view for cubic dose distribution estimated from the simulation of the GEVI system for the shifting scenarios considered in the present study. Spot sizes are proportional to the number of protons. The areas of local shift are marked with the black line. For each energy layer, the layer-averaged range shifts ± standard deviations (1σ) are given.

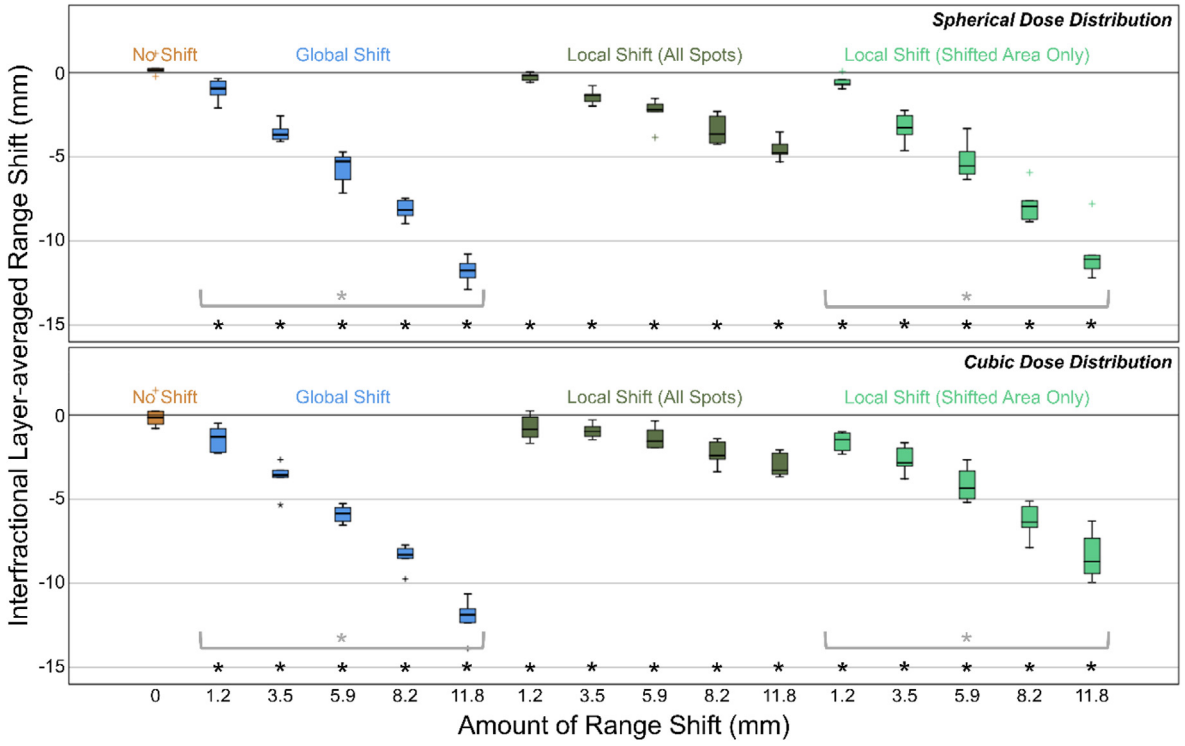

Fig. 5. Distribution of interfractional layer-averaged range shifts for spherical dose distribution (top) and cubic dose distribution (bottom). Significant differences as results of statistical hypothesis tests are marked with asterisks (gray for ANOVA tests and black for one-sided t-tests).

Table 1
Overall accuracy and precision for range shifting scenarios.

Range Shift Scenario		Accuracy [mm]	Precision [mm]
No Shift		0.01	0.39
Global Shift	11.8 mm	0.53	0.58
	8.2 mm	0.22	0.62
	5.9 mm	0.45	0.52
	3.5 mm	0.23	0.49
	1.2 mm	0.13	0.40
Local Shift (All Spots)	11.8 mm	8.24	1.70
	8.2 mm	5.34	1.29
	5.9 mm	4.18	0.90
	3.5 mm	2.46	0.72
	1.2 mm	0.79	0.45
Local Shift (Shifted Area Only)	11.8 mm	2.71	0.93
	8.2 mm	1.55	0.66
	5.9 mm	1.86	0.46
	3.5 mm	0.85	0.41
	1.2 mm	0.40	0.39

trajectories of the electrons, and the calorimeter measures the energy of the electrons. Detailed information on the GEVI system can be found elsewhere [20,21].

2.2. Treatment planning

Spot scanning proton treatment was planned for two simple dose distributions (i.e., cubic and spherical) in a cubic homogeneous PMMA phantom ($150 \times 150 \times 150$ mm^3). The treatment planning was conducted by using the Eclipse 13.7 treatment planning system (Varian Medical Systems, Palo Alto, CA) with relative biological effectiveness of 1.1 and range uncertainty margin of 3.5% + 1 mm. For the cubic dose distribution, a $50 \times 50 \times 50$ mm^3 cubic target volume was defined in the PMMA phantom and 1 Gy field dose was assumed to be delivered to the target volume, using total 12 energy layers ranging from 115.8 MeV to 149.1 MeV. For the spherical dose distribution, a spherical target volume of 80 mm diameter was defined in the PMMA phantom and 1 Gy field dose was assumed to be delivered to the target volume using total 18 energy layers from 104.8 MeV to 154.8 MeV. The isocenters of both dose distributions were located 50 mm away from the phantom center (0, 0, 50 mm).

2.3. Monte Carlo simulation

The measurement of PGs using the GEVI system was simulated with a Monte Carlo simulation toolkit, Geant4 (ver.10.04.p02) [22]. Fig. 1 shows the Geant4 model of the GEVI system in place to

measure the PGs from the PMMA phantom. In simulations, the spot scanning proton beams were delivered to the target volume in the PMMA phantom. The distance between the GEVI system and the target volume was 70 mm, and the system was positioned at the middle of the beam ranges of the distal six energy layers (i.e., 121.5 mm for cubic dose distribution and 130.2 mm for spherical dose distribution). For the distal six energy layers, the average numbers of protons per spot were 2.56×10^7 and 1.62×10^7 for cubic and spherical dose distributions, respectively. For hadronic physics process, we used the QGSP_BIC_HP modular physics list which is recommended for medical applications [23]. The cut values for proton, gamma, electron, and positron were set as 1.0 mm. The geometry of beam nozzle was not modeled, instead the proton pencil beam was irradiated 60 cm away from the isocenter with considering the beam spread and struggling.

2.4. Considered range shifts

Interfractional range shifts were simulated by placing a PMMA range shifting plate in the path of the proton beam. The shifts were classified into two groups: global and local shifts. To introduce a global shift, a large PMMA plate (150×150 mm^2) were placed on the proximal side of the phantom so that all spots in the target volume are affected by the plate (see Fig. 1). To introduce a local shift, a small PMMA plate was placed on the proximal side of the phantom so that only some portion of the spots in the target volume are affected by the plate. For the cubic dose distribution, a small square plate (25×25 mm^2) with varying thickness was placed at the center of the isocentric axis (see Fig. 2, left) to affect the spots at the central part of the target volume. For the spherical dose distribution, a small disk plate of 60 mm diameter with varying thickness was placed at 30 mm away from the isocenter (see Fig. 2, right). The thicknesses of the PMMA range shifting plate were 1, 3, 5, 7, and 10 mm, which correspond to 1.19, 3.52, 5.88, 8.24, and 11.75 mm range shifts, respectively. Furthermore, the proton ranges without the range shifting plate (i.e., no shift scenario) were also verified to prove the feasibility of the GEVI system.

2.5. Estimation of range shifts

The range shift detection is very sensitive to Poisson noise in the PG distribution, and a better precision can be achieved by using a larger number of protons. To improve PG statistics, therefore, it was assumed that neighboring spots in a given energy layer are aggregated with two-dimensional Gaussian smoothing ($\sigma = 7.8$ mm) where each spot is substituted by the sum of the spots in neighbor, including itself, based on the Gaussian-weights on their respective distance and their proton number [24,25]. This approach, called as spot aggregation, improves statistics at the cost of degradation in lateral spatial resolution. In the present study, the Gaussian-weighted aggregation with 7.8 mm σ was used, which has only a limited impact on lateral spatial resolution [18].

For each spot, interfractional range shift was analyzed by comparing two GEVI images (i.e., with and without shift). For each GEVI image, a projection image was produced by projecting the GEVI image on the X axis of the image which is parallel to the beam direction. The centroid of the projection image was then calculated using Equation (1) for two GEVI images (i.e., with and without shift) for each spot, and the difference of the two centroids is considered as the amount of range shift.

$$Centroid = \frac{\sum h_x x}{\sum h_x}, \quad \text{(Eq. 1)}$$

where h_x is the number of counts at position x on the X axis.

2.6. Statistical hypothesis tests

Statistical hypothesis tests were applied to the estimated range shifts [24]. To see if the different interfractional range shifting scenarios are distinguishable from one another, one-way ANOVA (analysis of variance) tests were used. One-way ANOVA test is widely used in the analysis of difference between more than two categories of data. For the ANOVA test, in the present study, the null hypothesis was that the difference between the shifting scenarios is not statistically significant. Additionally, the differences of each shifting from zero shifting were tested with one-sample t-tests in order to estimate shift detection sensitivity. One-sample *t*-test is generally applied to test whether a population mean is significantly different from some hypothesized value. For the *t*-test, in the present study, the null hypothesis was defined as no difference between the population mean of shifting scenarios and zero. The p-values resulting from the hypothesis tests were compared to the 5% significance level, and the null hypothesis was rejected only when the p-value is lower than the significance level. All statistical hypothesis tests were conducted using SPSS 25 (IBM, Armonk, NY).

3. Results and discussion

Figs. 3 and 4 show the maps of the interfractional range shifts in the beam's eye view, for spherical and cubic dose distributions, respectively, which were estimated from Geant4 simulations for the shifting scenarios. In the range shift maps, the estimated range shifts are presented in their spot positions, and the spot sizes are proportional to the number of protons. For the local shifts, the shifted area is marked with a black line. For each map, the layer-averaged range shifts and their standard deviations (1σ) are also given; for the local shifts, the layer-averaged range shifts were calculated in two ways: (1) using all spots in the energy layer and (2) using only the spots affected by the range shifting (i.e., in the black line).

For the no shifting and global shifting scenarios, the introduced shifts were clearly observed in all energy layers. Most of the evaluated range shifts were within 1 mm error. However, relatively larger statistical fluctuations were found in the proximal energy layers. From the most three distal energy layers, the standard deviations were lower than 1 mm, whereas for the most three proximal layers, the standard deviations were larger than 1 mm. It was mainly due to smaller number of protons delivered to the spots in the proximal energy layers. For the local shifting scenarios, the range shifts were estimated with lower accuracy and precision compared to the no shifting and global shifting cases. The errors were as large as a few millimeters. Nevertheless, significantly better results were obtained if only the shifted area was considered. However, the evaluated local shifts still suffered from low accuracy because the shifted and non-shifted ranges were mixed after the spot aggregation especially near the shift boundary (i.e., range mixing effect).

Fig. 5 shows the box plots of the distribution of estimated interfractional layer-averaged range shifts with the results of statistical hypothesis tests. For the no shifting and global shifting scenarios, the estimated range shifts tend to be close to the true shifts. Considering the average values, the maximum errors were about 1.15 and 2.14 mm for the 10 mm shifting scenario in the spherical and cubic dose distributions, respectively. For the local shifting scenarios, when we consider all spots in the energy layers, the estimated layer-averaged range shifts show very large errors when compared to the results of the global shifting scenarios. The maximum errors were as large as ~8 mm for the 10 mm shifting scenarios. However, the errors were found to be significantly decreased when we considered only the spots affected by the range

shifting.

For each statistical hypothesis test, the significant differences (i.e., differences from other shifting scenarios and from zero shifting for ANOVA tests and one-sided t-tests, respectively) are marked with an asterisk: gray for ANOVA tests and black for one-sided t-tests. For the global shifting scenarios, the results of the ANOVA tests show that the differences between the results of the global shifting scenarios were all statistically significant, which shows that all global shifting scenarios were distinguishable from one another. For the local shifting scenarios, ANOVA tests were performed only for the scenarios where we consider only the spots which were affected by the local shifting (i.e., using the spots in the black line). The results again show that the differences between the results of the local shifting scenarios were all statistically significant, which shows that all local shifting scenarios were distinguishable from one another. One-sided t-tests were performed for all shifting scenarios, and the results show that all shifting scenarios, expect no shift, were differed significantly from zero shifting, which indicates that the interfractional range shift can be detected down to 1 mm, even if the local shifted area is unknown.

Table 1 shows the overall accuracy and precision for all investigated scenario cases. The accuracies were calculated as the difference between the estimated range shift and the true shift (= introduced shift), and the precisions were calculated as 1.5 times of the standard deviation (σ). Note that this 1.5 σ is used to compare with the distal safety margin [1]. In Table 1, for the no shift and global shift scenarios, both accuracies and precisions were acceptable with the difference smaller than 1 mm. The results showed that a high performance of the GEVI system can be expected especially for no shifting and global shifting cases. For the local shift scenarios, relatively low accuracies and precisions were found for both all spots and shifted area only. The accuracy and precision were increased with the shifting magnitude, which was mainly due to range mixing effect, originated from the spot aggregation, near the local shift boundary. More significant range mixing occurred for larger range difference between the shifted and non-shifted spots, and this increased accuracy and precision of the local shifts. Meanwhile, the precisions were less than 1.70 mm for all cases; furthermore, they came to be smaller than ~1 mm if the shifted area was known (i.e., no shift, global shifts, and local shift for shifted area only). These precision results were very encouraging for reduction of the range uncertainty, because the current distal safety margin is much larger than the precision of GEVI system. It should be noted that the smallest distal safety margin in the present study was 4.88 mm for 134.9 MeV by using the '3.5% + 1 mm' calculation. The distal safety margin is expected to be reduced if proton beam range is precisely monitored by the GEVI system.

4. Conclusion

In the present study, the performance of the GEVI system in spot scanning proton therapy was predicted by Geant4 Monte Carlo simulations. Two simplified cases of spot scanning proton treatment were considered, and several interfractional range shifts were introduced to the treatment cases assuming that the patient anatomy was changed between two neighboring fractions. The simulation results showed that the GEVI system can detect the interfractional range shifts down to 1 mm shift for the cases considered in the present study. The results also showed that both the accuracy and precision are less than 1–2 mm except for the local shift (all spots) cases, which was very encouraging considering that it is significantly lower than the smallest distal safety margin of the investigated beam energy (i.e., 4.88 mm for 134.9 MeV from the '3.5% + 1 mm' calculation). The results of the present study generally indicated that the GEVI system is a very promising system for *in-vivo* range verification in proton therapy.

Declaration of competing interest

The authors declare that they have no known competing financial interests or personal relationships that could have appeared to influence the work reported in this paper.

Acknowledgements

This research was supported by the National Cancer Center Grants (NCC-2110390-2), Korea.

References

[1] H. Paganetti, Range uncertainties in proton therapy and the role of Monte Carlo simulations, Phys. Med. Biol. 57 (2012), https://doi.org/10.1088/0031-9155/57/11/R99.
[2] A.C. Knopf, A. Lomax, In vivo proton range verification: a review, Phys. Med. Biol. 58 (2013) 131–160, https://doi.org/10.1088/0031-9155/58/15/R131.
[3] L. Sulak, T. Armstrong, H. Baranger, M. Bregman, M. Levi, D. Mael, J. Strait, T. Bowen, A.E. Pifer, P.A. Polakos, H. Bradner, A. Parvulescu, W.V. Jones, J. Learned, Experimental studies of the acoustic signature of proton beams traversing fluid media, Nucl. Instrum. Methods 161 (1979) 203–217, https://doi.org/10.1016/0029-554X(79)90386-0.
[4] S.C. Krejcarek, P.E. Grant, J.W. Henson, N.J. Tarbell, T.I. Yock, Physiologic and radiographic evidence of the distal edge of the proton beam in craniospinal irradiation, Int. J. Radiat. Oncol. Biol. Phys. 68 (2007) 646–649, https://doi.org/10.1016/j.ijrobp.2007.02.021.
[5] M. Yamaguchi, K. Torikai, N. Kawachi, H. Shimada, T. Satoh, Y. Nagao, S. Fujimaki, M. Kokubun, S. Watanabe, T. Takahashi, K. Arakawa, T. Kamiya, T. Nakano, Erratum: beam range estimation by measuring bremsstrahlung (physics in medicine and biology (2012) 57 (2843, Phys. Med. Biol. 61 (2016) 3638–3644, https://doi.org/10.1088/0031-9155/61/9/3638.
[6] K. Parodi, T. Bortfeld, Physics in Medicine & Biology Related Content Proton Dose Monitoring with PET : Quantitative Studies in Lucite Proton Dose Monitoring with PET : Quantitative Studies in Lucite, 1996.
[7] C.H. Min, C.H. Kim, M.Y. Youn, J.W. Kim, Prompt gamma measurements for locating the dose falloff region in the proton therapy, Appl. Phys. Lett. 89 (2006) 2–5, https://doi.org/10.1063/1.2378561.
[8] A.C. Kraan, Range verification methods in particle therapy: underlying physics and Monte Carlo modelling, Front. Oncol. 5 (2015) 1–27, https://doi.org/10.3389/fonc.2015.00150.
[9] K. Parodi, On- and off-line monitoring of ion beam treatment, Nucl. Instrum. Methods Phys. Res. Sect. A Accel. Spectrom. Detect. Assoc. Equip. 809 (2016) 113–119, https://doi.org/10.1016/j.nima.2015.06.056.
[10] J. Krimmer, D. Dauvergne, J.M. Létang, Testa, Prompt-gamma monitoring in hadrontherapy: a review, Nucl. Instrum. Methods Phys. Res. Sect. A Accel. Spectrom. Detect. Assoc. Equip. 878 (2018) 58–73, https://doi.org/10.1016/j.nima.2017.07.063.
[11] J. Smeets, F. Roellinghoff, D. Prieels, F. Stichelbaut, A. Benilov, P. Busca, C. Fiorini, R. Peloso, M. Basilavecchia, T. Frizzi, J.C. Dehaes, A. Dubus, Prompt gamma imaging with a slit camera for real-time range control in proton therapy, Phys. Med. Biol. 57 (2012) 3371–3405, https://doi.org/10.1088/0031-9155/57/11/3371.
[12] D. Kim, H. Yim, J.W. Kim, Pinhole camera measurements of prompt gamma-rays for detection of beam range variation in proton therapy, J. Kor. Phys. Soc. 55 (2009) 1673–1676, https://doi.org/10.3938/jkps.55.1673.
[13] D.B. Everett, J.S. Fleming, R.W. Todd, J.M. Nightingale, Gamma-radiation imaging system based on the Compton effect, Proc. Inst. Electr. Eng. 124 (1977) 995–1000, https://doi.org/10.1049/piee.1977.0203.
[14] C. Golnik, F. Hueso-González, A. Müller, P. Dendooven, W. Enghardt, F. Fiedler, T. Kormoll, K. Roemer, J. Petzoldt, A. Wagner, G. Pausch, Range assessment in particle therapy based on prompt γ-ray timing measurements, Phys. Med. Biol. 59 (2014) 5399–5422, https://doi.org/10.1088/0031-9155/59/18/5399.
[15] J. Krimmer, G. Angellier, L. Balleyguier, D. Dauvergne, N. Freud, J. Hérault, J.M. Létang, H. Mathez, M. Pinto, E. Testa, Y. Zoccarato, A cost-effective monitoring technique in particle therapy via uncollimated prompt gamma peak integration, Appl. Phys. Lett. 110 (2017), https://doi.org/10.1063/1.4980103.
[16] J.M. Verburg, H.A. Shih, J. Seco, Simulation of prompt gamma-ray emission during proton radiotherapy, Phys. Med. Biol. 57 (2012) 5459–5472, https://doi.org/10.1088/0031-9155/57/17/5459.
[17] C. Richter, G. Pausch, S. Barczyk, M. Priegnitz, I. Keitz, J. Thiele, J. Smeets, F. Vander Stappen, L. Bombelli, C. Fiorini, L. Hotoiu, I. Perali, D. Prieels, W. Enghardt, M. Baumann, First clinical application of a prompt gamma based in vivo proton range verification system, Radiother. Oncol. 118 (2016) 232–237, https://doi.org/10.1016/j.radonc.2016.01.004.
[18] Y. Xie, E.H. Bentefour, G. Janssens, J. Smeets, F. Vander Stappen, L. Hotoiu,

L. Yin, D. Dolney, S. Avery, F. O'Grady, D. Prieels, J. McDonough, T.D. Solberg, R.A. Lustig, A. Lin, B.K.K. Teo, Prompt gamma imaging for in vivo range verification of pencil beam scanning proton therapy, Int. J. Radiat. Oncol. Biol. Phys. 99 (2017) 210–218, https://doi.org/10.1016/j.ijrobp.2017.04.027.

[19] C.H. Kim, J.H. Park, H. Seo, H.R. Lee, Gamma electron vertex imaging and application to beam range verification in proton therapy, Med. Phys. 39 (2012) 1001–1005, https://doi.org/10.1118/1.3662890.

[20] C.H. Kim, H.R. Lee, S.H. Kim, J.H. Park, S. Cho, W.G. Jung, Gamma electron vertex imaging for in-vivo beam-range measurement in proton therapy: experimental results, Appl, Phys. Lett. 113 (2018), https://doi.org/10.1063/1.5039448.

[21] H.R. Lee, S.H. Kim, J.H. Park, W.G. Jung, H. Lim, C.H. Kim, Prototype system for proton beam range measurement based on gamma electron vertex imaging, Nucl. Instrum. Methods Phys. Res. Sect. A Accel. Spectrom. Detect. Assoc. Equip. 857 (2017) 82–97, https://doi.org/10.1016/j.nima.2017.03.022.

[22] J. Allison, K. Amako, J. Apostolakis, P. Arce, M. Asai, T. Aso, E. Bagli, A. Bagulya, S. Banerjee, G. Barrand, B.R. Beck, A.G. Bogdanov, D. Brandt, J.M.C. Brown, H. Burkhardt, P. Canal, D. Cano-Ott, S. Chauvie, K. Cho, G.A.P. Cirrone, G. Cooperman, M.A. Cortés-Giraldo, G. Cosmo, G. Cuttone, G. Depaola, L. Desorgher, X. Dong, A. Dotti, V.D. Elvira, G. Folger, Z. Francis, A. Galoyan, L. Garnier, M. Gayer, K.L. Genser, V.M. Grichine, S. Guatelli, P. Guèye, P. Gumplinger, A.S. Howard, I. Hřivnáčová, S. Hwang, S. Incerti, A. Ivanchenko, V.N. Ivanchenko, F.W. Jones, S.Y. Jun, P. Kaitaniemi, N. Karakatsanis, M. Karamitrosi, M. Kelsey, A. Kimura, T. Koi, H. Kurashige, A. Lechner, S.B. Lee, F. Longo, M. Maire, D. Mancusi, A. Mantero, E. Mendoza, B. Morgan, K. Murakami, T. Nikitina, L. Pandola, P. Paprocki, J. Perl, I. Petrović, M.G. Pia, W. Pokorski, J.M. Quesada, M. Raine, M.A. Reis, A. Ribon, A. Ristić Fira, F. Romano, G. Russo, G. Santin, T. Sasaki, D. Sawkey, J.I. Shin, I.I. Strakovsky, A. Taborda, S. Tanaka, B. Tomé, T. Toshito, H.N. Tran, P.R. Truscott, L. Urban, V. Uzhinsky, J.M. Verbeke, M. Verderi, B.L. Wendt, H. Wenzel, D.H. Wright, D.M. Wright, T. Yamashita, J. Yarba, H. Yoshida, Recent developments in GEANT4, Nucl. Instrum. Methods Phys. Res. Sect. A Accel. Spectrom. Detect. Assoc. Equip. 835 (2016) 186–225, https://doi.org/10.1016/j.nima.2016.06.125.

[23] H.Q. Tan, J.H. Phua, L. Tan, K.W. Ang, J. Lee, A.A. Bettiol, Geant4 simulation for commissioning of proton therapy centre, World Congr. Med. Phys. Biomed. Eng. (2018) 583–587, 2019.

[24] L. Nenoff, M. Priegnitz, G. Janssens, J. Petzoldt, P. Wohlfahrt, A. Trezza, J. Smeets, G. Pausch, C. Richter, Sensitivity of a prompt-gamma slit-camera to detect range shifts for proton treatment verification, Radiother. Oncol. 125 (2017) 534–540, https://doi.org/10.1016/j.radonc.2017.10.013.

[25] S.H. Kim, J.H. Park, Y. Ku, H.S. Lee, Y. Kim, C.H. Kim, J.H. Jeong, Improvement of statistics in proton beam range measurement by merging prompt gamma distributions: a preliminary study, J. Radiat. Prot. Res. (2019), https://doi.org/10.14407/jrpr.2019.44.1.1.